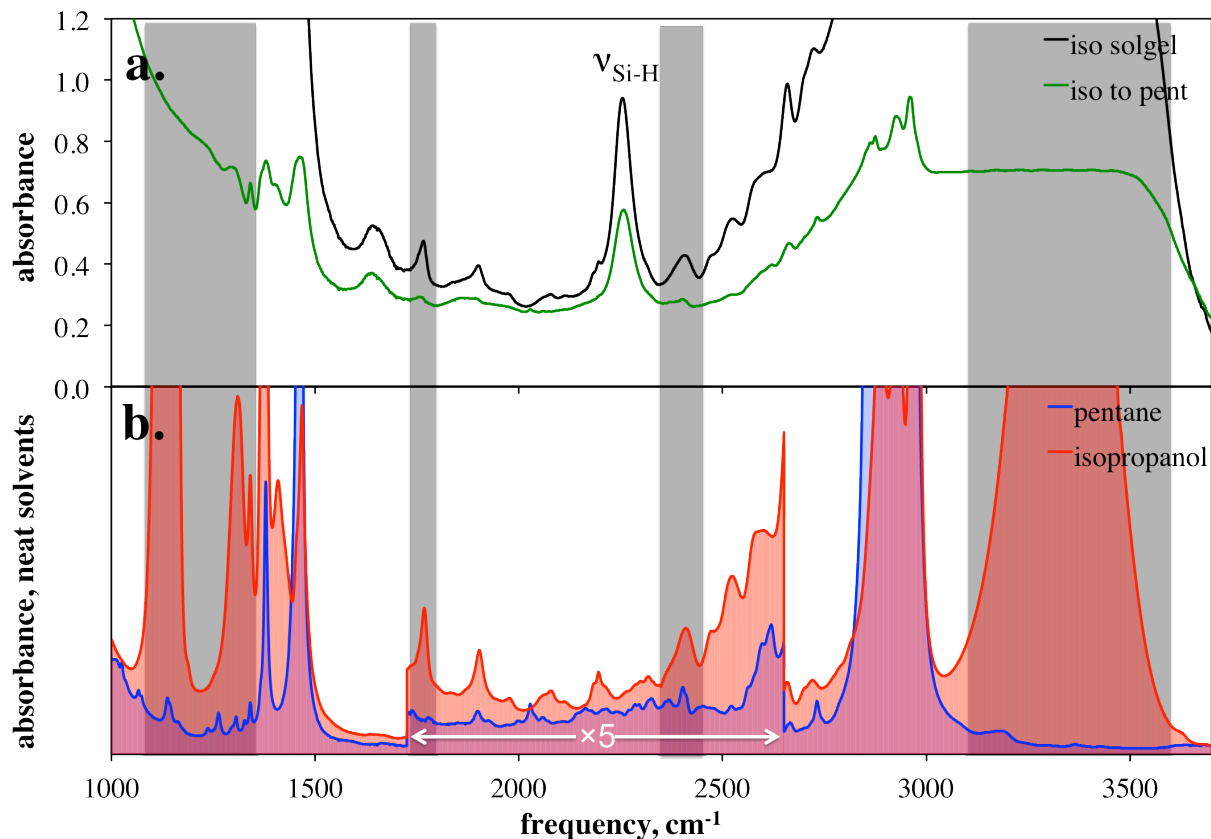# Supporting Information for:

# Characterizing Solvent Dynamics in Nanoscopic Silica Sol-Gel Glass Pores by 2D-IR Spectroscopy of an Intrinsic Vibrational Probe

*Christopher J. Huber and Aaron M. Massari\**

Department of Chemistry, University of Minnesota – Twin Cities

207 Pleasant St SE, Minneapolis, MN 55455

*Corresponding author. Email: massari@umn.edu

**Figure S1.** a) Raw FTIR spectra for a silica alcogel infiltrated with isopropanol (black) and then soaked in pentane for four days to exchange the solvent (green). b) Neat solvent spectra for isopropanol (red) and pentane (blue) are shown for reference. The middle section of this plot is scaled by a factor of five to clarify the smaller solvent peaks in this region. Note that in a) the silica sol-gel has significant absorbance below 1500 cm$^{-1}$ and above 3000 cm$^{-1}$ making it difficult to see changes in these regions. Gray boxes have been overlaid to highlight some of the salient points. Below 1500 cm$^{-1}$ and above 3000 cm$^{-1}$ there are clear enhancements in absorbance for the isopropanol sol-gel, although these quickly become off-scale and hard to quantify. The spectral region of 1750 cm$^{-1}$ and 2400 cm$^{-1}$ highlight isopropanol peaks that are present in the isopropanol sol-gel but absent (or notably changed) for the pentane case. This demonstrates that the majority of the volume of the sol-gel pores is infiltrated with pentane.
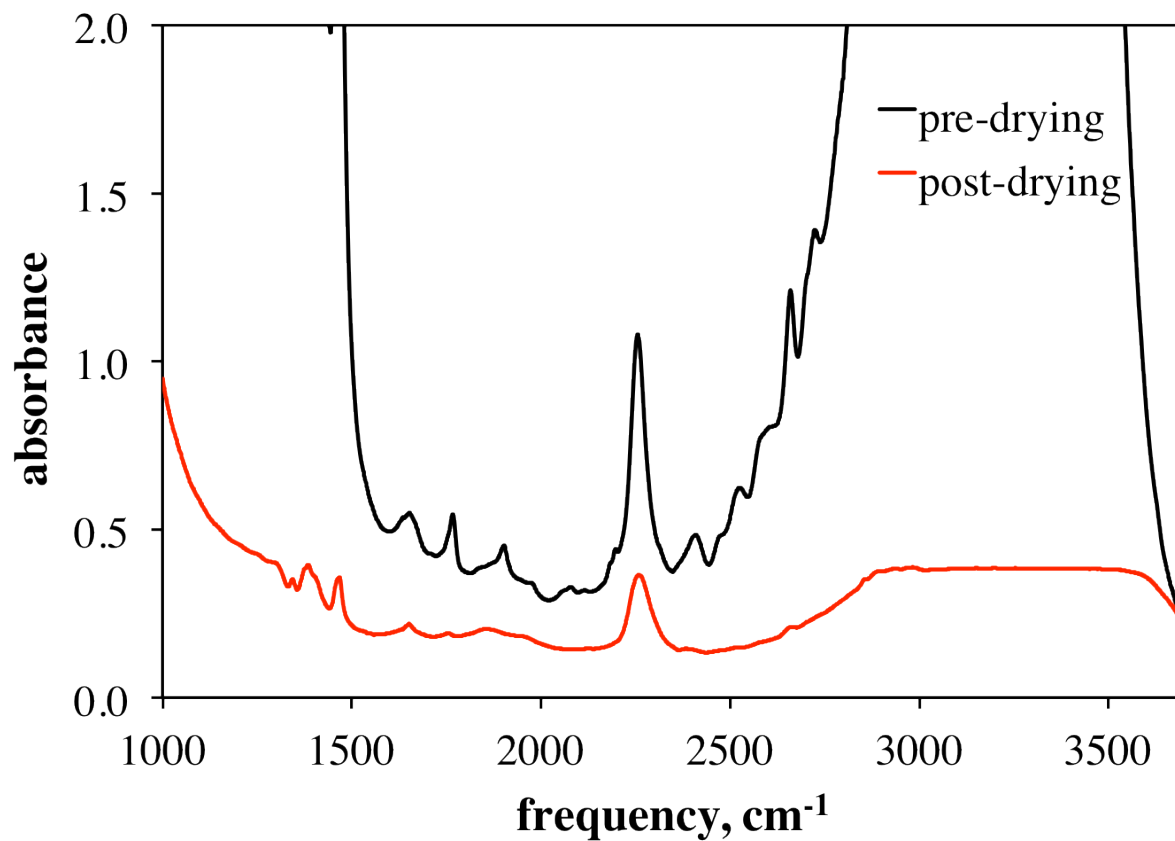
**Figure S2.** Raw FTIR spectra of an isopropanol alcogel before (black) and after supercritical $CO_2$ drying (red). Note that although there is a lot of persistent absorbance by the silica, the majority of the solvent peaks through the 1500 cm$^{-1}$ to 2700 cm$^{-1}$ range are absent after drying, indicating that the solvent has been removed.
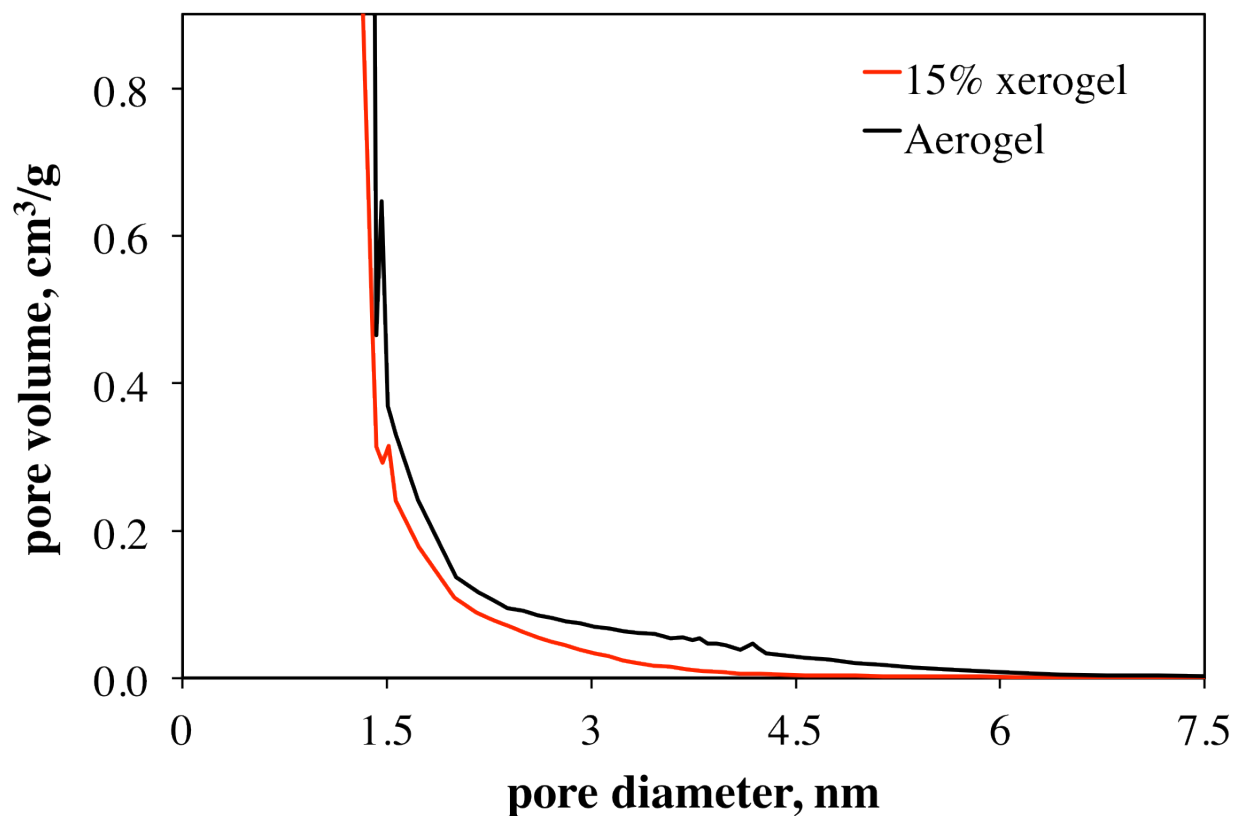
**Figure S3.** Pore volume as a function of pore diameter using a BJH analysis of the $N_2$ adsorption isotherms shown in Figure 2. Both the aerogel and xerogel samples have a very high percentage of the pore volume that corresponds to pore diameters <1.5 nm, unfortunately that region is not resolvable with the use of $N_2$ gas. It should be noted that the aerogel sample does show a broad pore distribution at around 3.75 nm, which could indicate another pore regime that collapses in the xerogel sample.
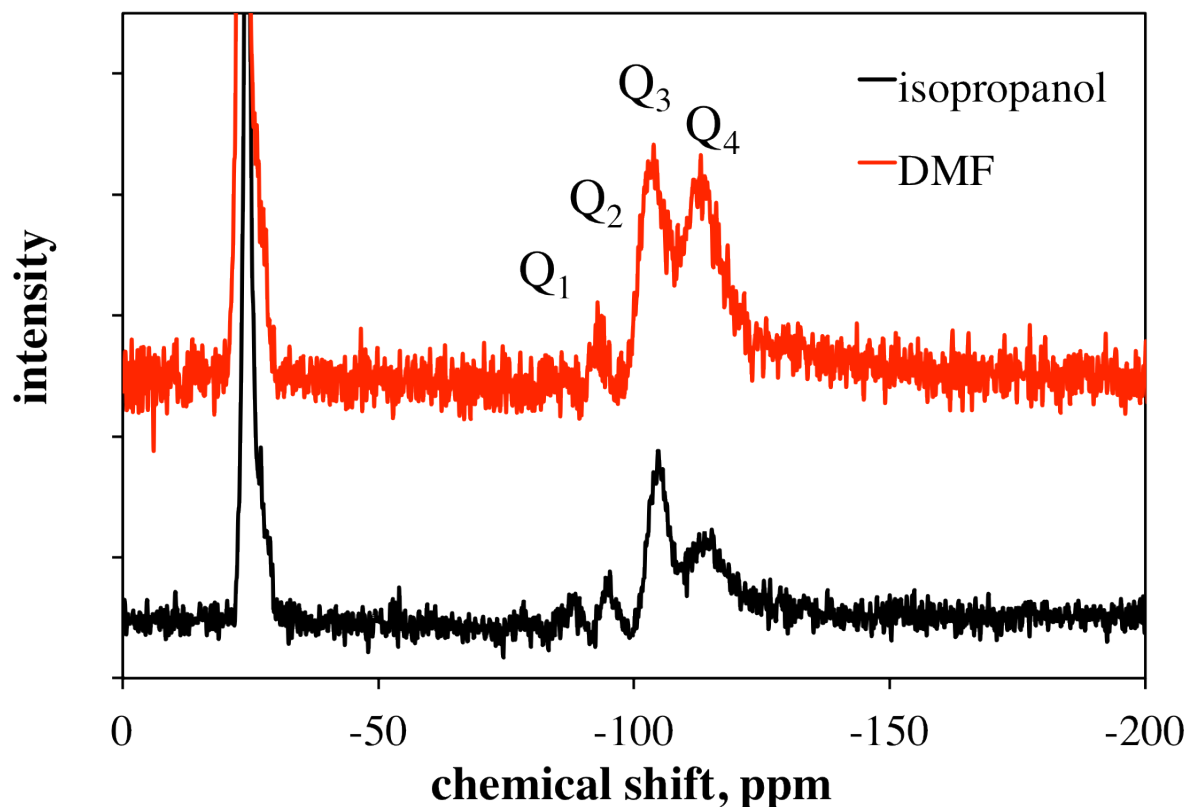
**Figure S4.** Solid-state Si$^{29}$ NMR spectra of xerogel samples (vacuum dried alcogels) that were synthesized with isopropanol (black) and DMF (red) as the infiltrating solvents. The peaks at -86, -95, -104, and -112 ppm are assigned as the $Q_1$, $Q_2$, $Q_3$, and $Q_4$ peaks, respectively.[1-3] These peaks correspond to $(SiO)Si(OR)_3$, $(SiO)_2Si(OR)_2$, $(SiO)_3Si(OR)$, and $(SiO)_4Si$, respectively, where R is either H or $CH_3$.[1-3] We do not see evidence for the $Q_0$ peak. The silicon atoms in sol-gels infiltrated with both solvents are mostly tertiary and quaternary coordinated and highly cross-linked. The integrated peak areas are: (isopropanol) $Q0 = 3.7\%$, $Q_1 = 6.5\%$, $Q_2 = 8.3\%$, $Q_3 = 38.7\%$, $Q_4 = 42.8\%$; and (DMF) $Q_1 = 4.5\%$, $Q_2 = 6.5\%$, $Q_3 = 36.7\%$, $Q_4 = 52.2\%$.
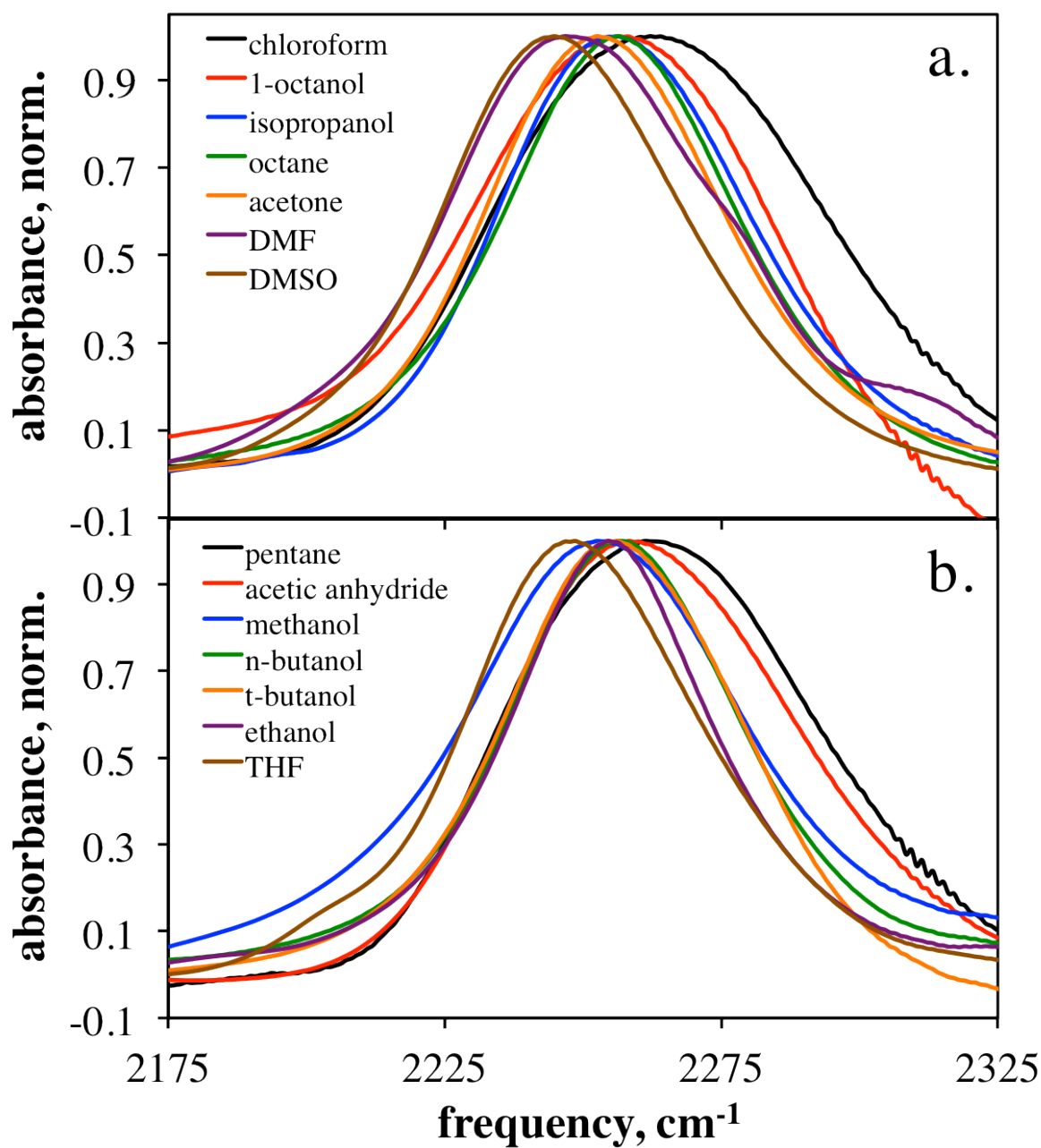
**Figure S5.** Baselined, solvent subtracted, and normalized FTIR spectra of the $\nu_{Si-H}$ region for silica alcogels infiltrated with all solvents examined in this study. Frames a) and b) show two groups of samples arbitrarily separated for clarity. These spectra were analyzed to produce the $\nu_{Si-H}$ values in Figures 5 and S6 as well as the center $\nu_{Si-H}$ and FWHMs in Table S1.

**Table S1.** Solvent parameters and corresponding silane vibrational mode characteristics.

| solvent | $\nu_{Si-H}$ (cm$^{-1}$)[c] | FWHM (cm$^{-1}$) | $\alpha$ [a] | $\beta$ [a] | $\pi$*[a] | $\delta$ |
|---|---|---|---|---|---|---|
| DMSO | 2244.6 | 51.8 | 0 | 0.76 | 1 | 0 |
| DMF | 2247.8 | 60.3 | 0 | 0.69 | 0.88 | 0 |
| THF | 2248.1 | 49.2 | 0 | 0.55 | 0.58 | 1 |
| acetone | 2252.8 | 50.8 | 0.08 | 0.43 | 0.71 | 0 |
| methanol | 2253.1 | 58.6 | 0.98 [a] <br> 0.35 [b] | 0.66 [a] <br> 0.46 [b] | 0.60 [a] <br> 0.35 [b] | 0 |
| ethanol | 2254.8 | 42.3 | 0.86 [a] <br> 0.29 [b] | 0.75 [a] <br> 0.52 [b] | 0.54 [a] <br> 0.29 [b] | 0 |
| t-butanol | 2255.6 | 49.3 | 0.42 [a] <br> 0.31 [b] | 0.93 [a] <br> 0.52 [b] | 0.41 [a] <br> 0.30 [b] | 0 |
| isopropanol | 2255.6 | 52.9 | 0.76 [a] <br> 0.29 [b] | 0.84 [a] <br> 0.51 [b] | 0.48 [a] <br> 0.21 [b] | 0 |
| octane | 2256.3 | 49.8 | 0 | 0 | 0.01 | 0 |
| n-butanol | 2256.6 | 48.8 | 0.84 [a] <br> 0.84 [b] | 0.84 [a] <br> 0.84 [b] | 0.47 [a] <br> 0.47 [b] | 0 |
| 1-octanol | 2256.7 | 61.6 | 0.77 [a] <br> 0.35 [b] | 0.81 [a] <br> 0.51 [b] | 0.40 [a] <br> 0.36 [b] | 0 |
| acetic anhydride | 2258.9 | 59.6 | 0 | 0.29 | 0.76 | 0 |
| chloroform | 2262.5 | 69.0 | 0.2 | 0.1 | 0.58 | 0.5 |
| pentane | 2262.6 | 63.9 | 0 | 0 | -0.08 | 0 |
| TMOS | 2199.2 | 66.3 | | | | |
| P-I-P-HighV(1) | 2257.9 | 54.7 | | | | |
| aerogel | 2260.9 | 63.2 | | | | |

a) Values from reference 4, unless otherwise noted.

b) Values from reference 5.

c) The FTIR spectra in each solvent were carried out in triplicate and the errors in FWHW and peak centers for each solvent were always within the resolution of the FTIR, see Experimental Section.
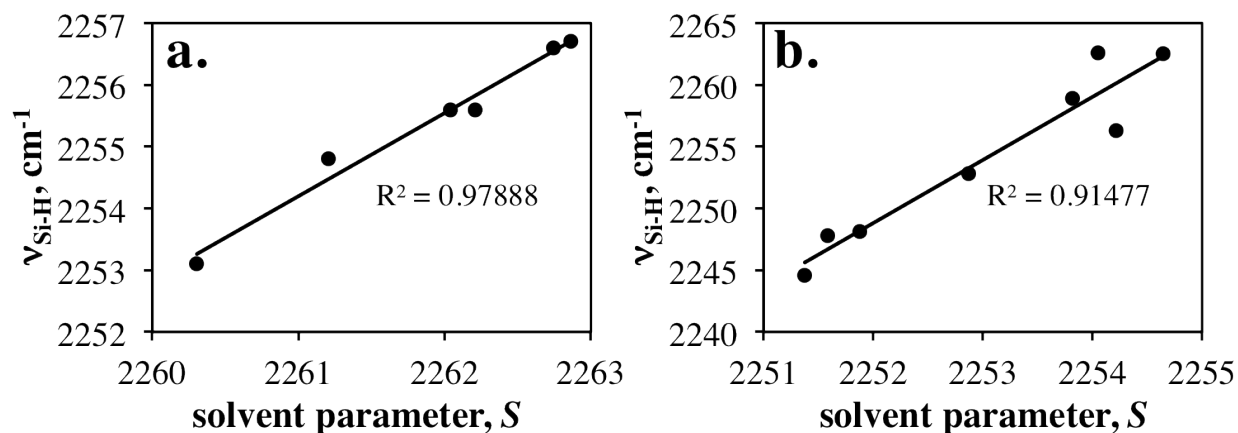
**Figure S6.** LSER analysis of solvatochromic shifts of the $\nu_{Si-H}$ treating separately the a) alcohols and b) non-alcohols using Marcus' parameters for both correlation plots (not Carr alcohols).[4,5] The high correlation obtained when separating these solvent types demonstrates that Marcus parameters do capture the correlation between solvent properties and spectral shifts, but are not internally consistent for these solvent categories.
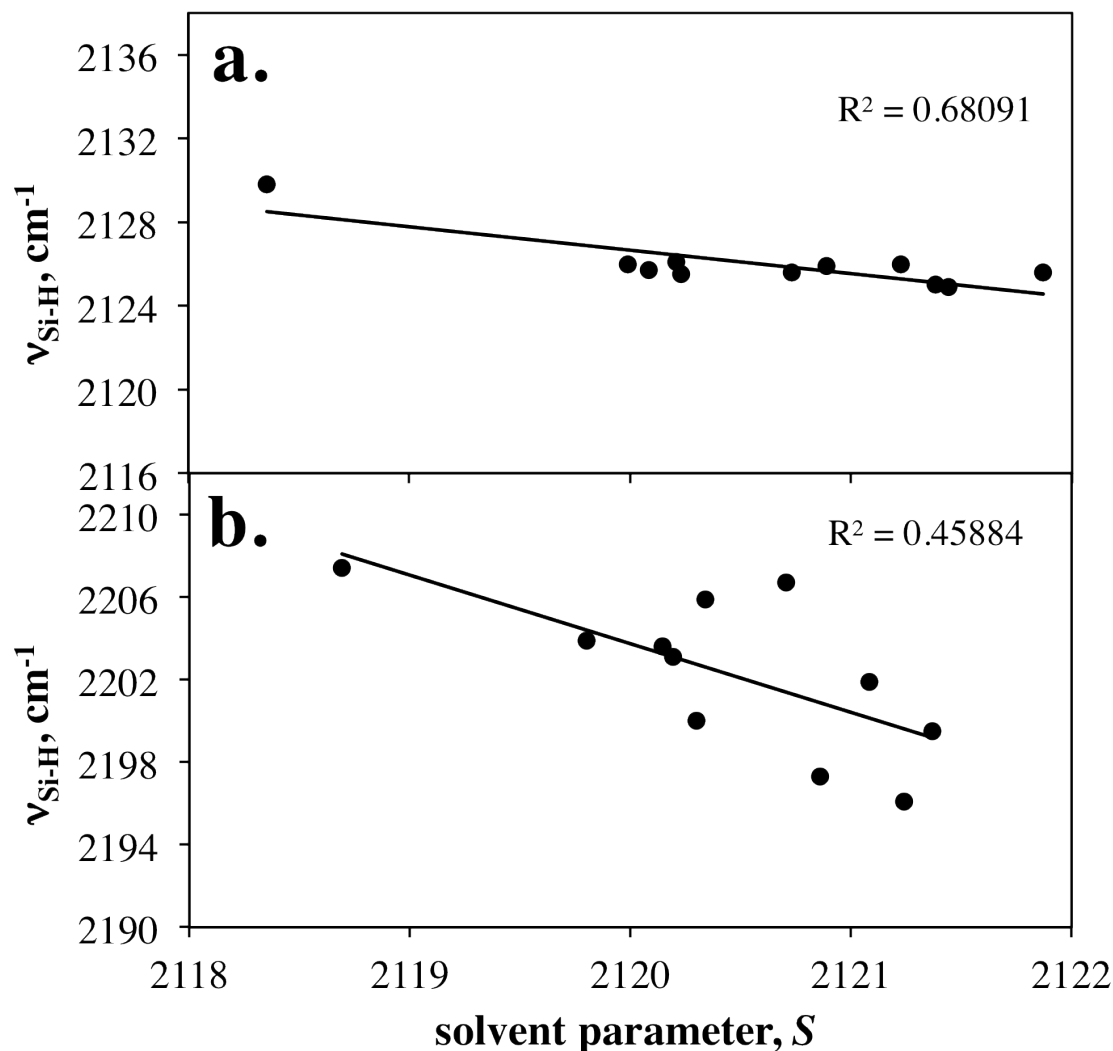
**Figure S7.** Solvatochromic shifts of $\nu_{Si-H}$ on a) triphenylsilane (TriPS) and b) TriMOS precursor. The y-axis scales are both 22 cm$^{-1}$, which is the same as Figure 5 so that the extent of solvatochromism can be compared. The $\nu_{Si-H}$ on TriPS is notably insensitive to the solvent and shifts by only a few wavenumbers. The $\nu_{Si-H}$ on TriMOS is solvatochromic on the scale of the silica, though the correlation between the solvent parameter is not as conclusive as Figure 5. The TriPS lacks the oxygen atoms and hydroxyl groups adjacent to the silicon to serve as hydrogen bond acceptors and donors, which appears to correlate with the loss of solvent sensitivity. We conclude from this that the frequency shifts are due in large part to the oxygen atoms in the silica matrix.
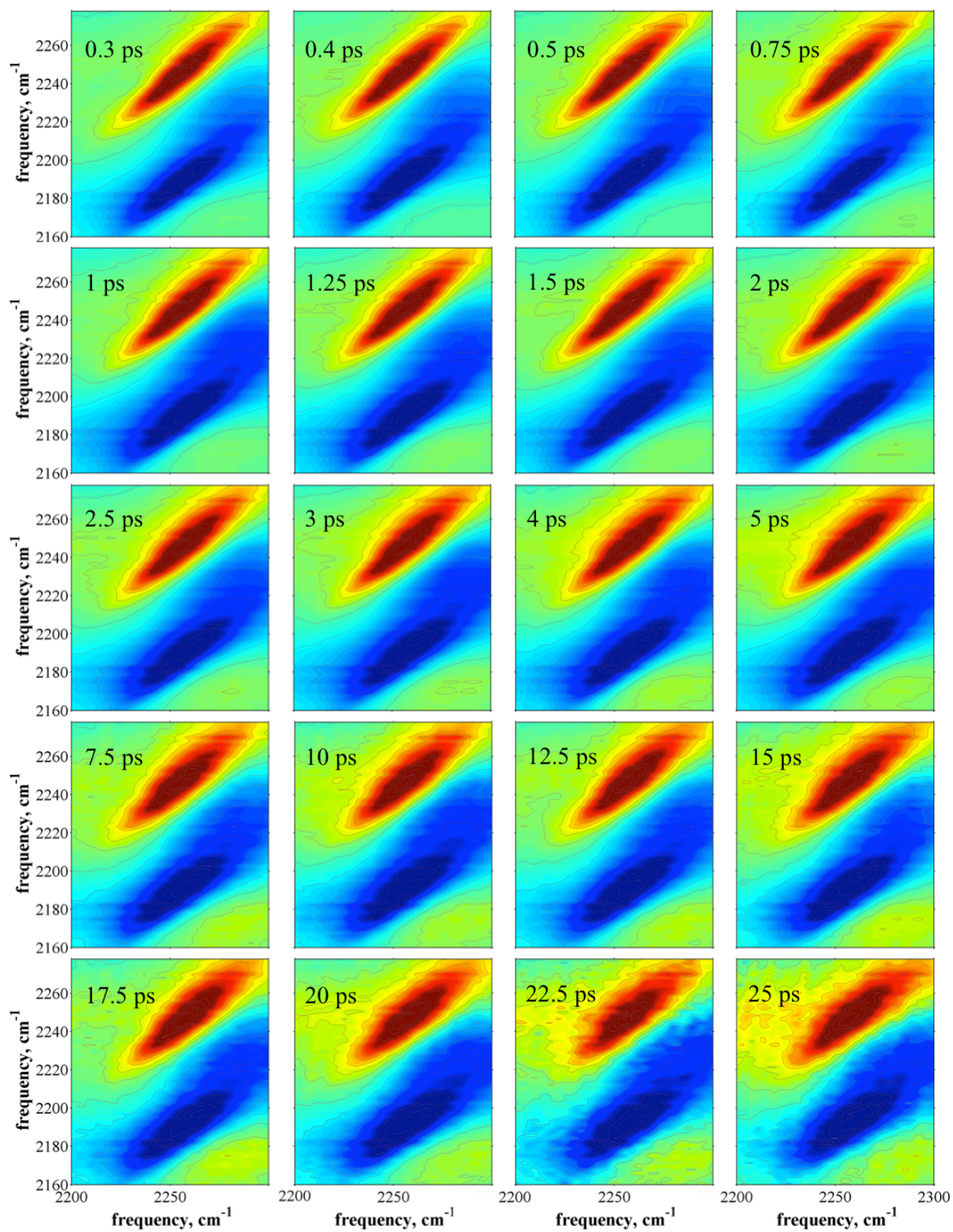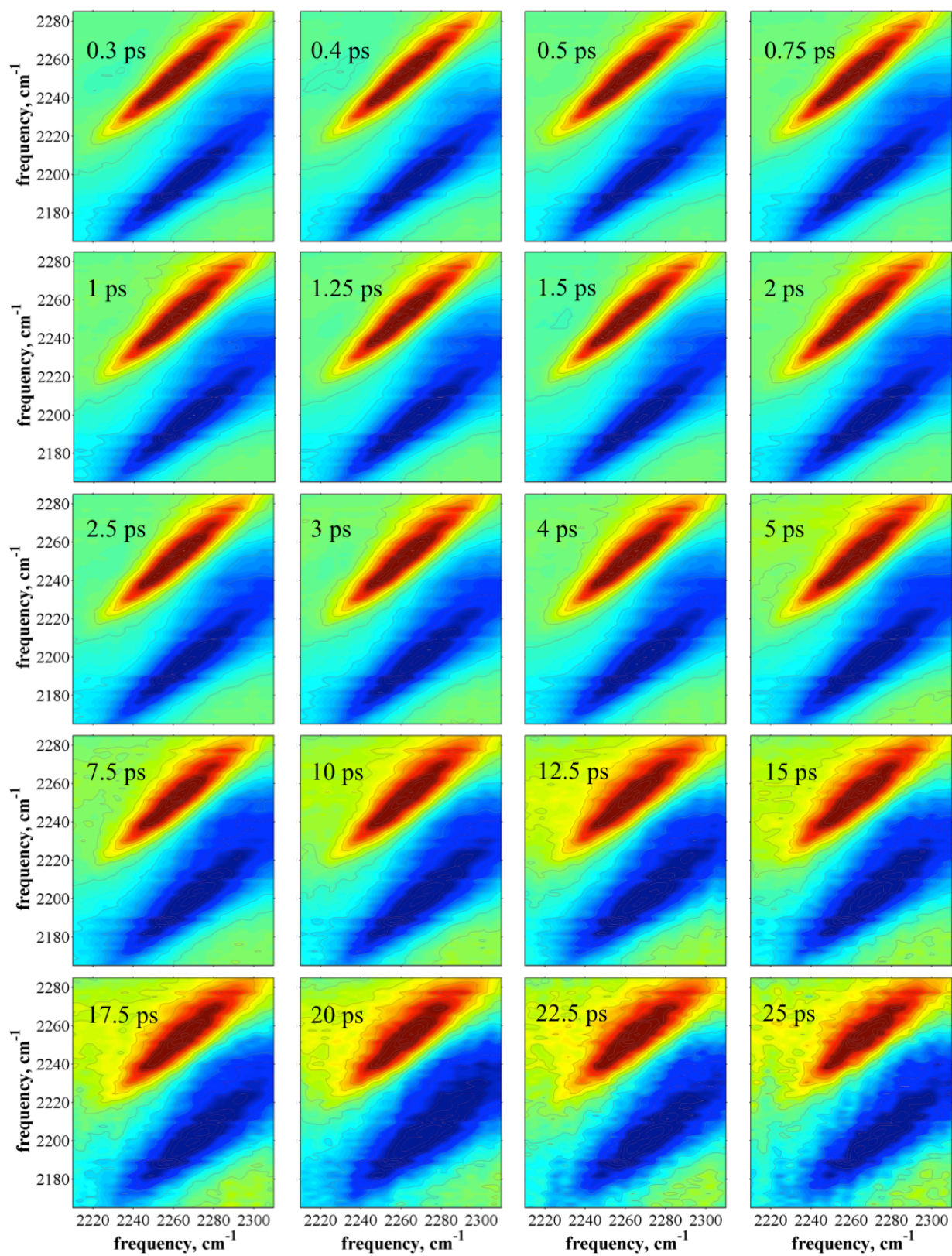
**Figure S8.** 2D-IR spectra for isopropanol infiltrated alcogel.
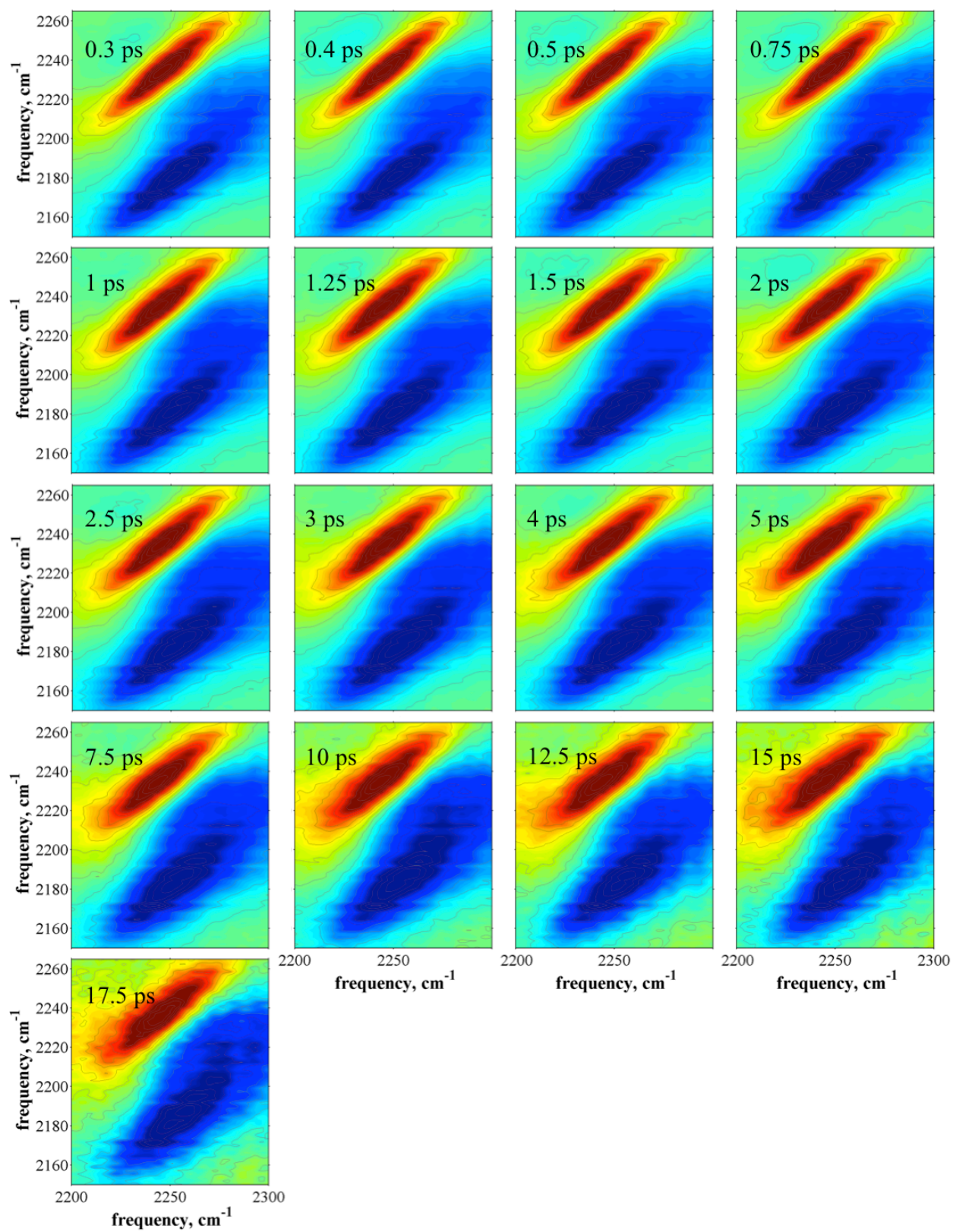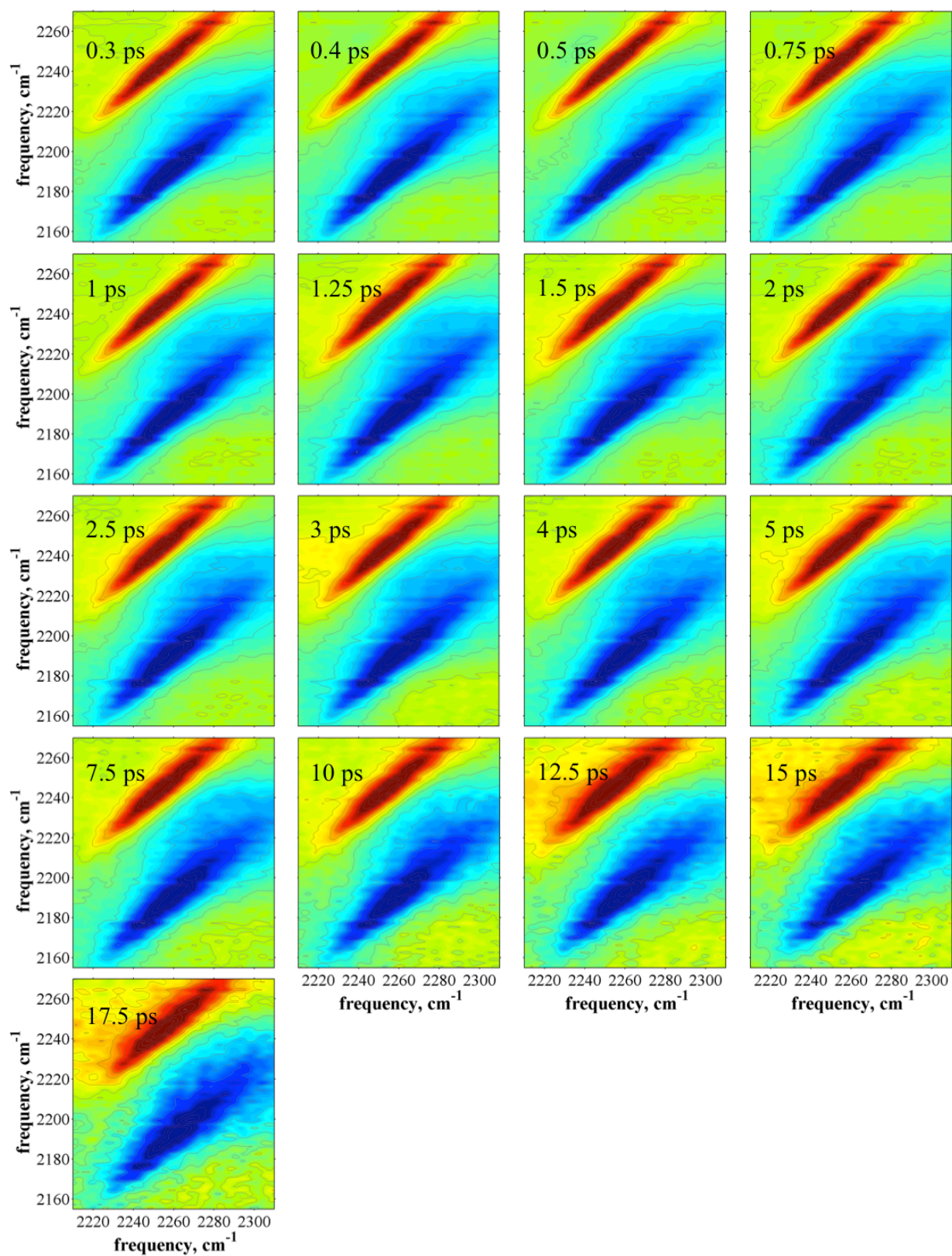
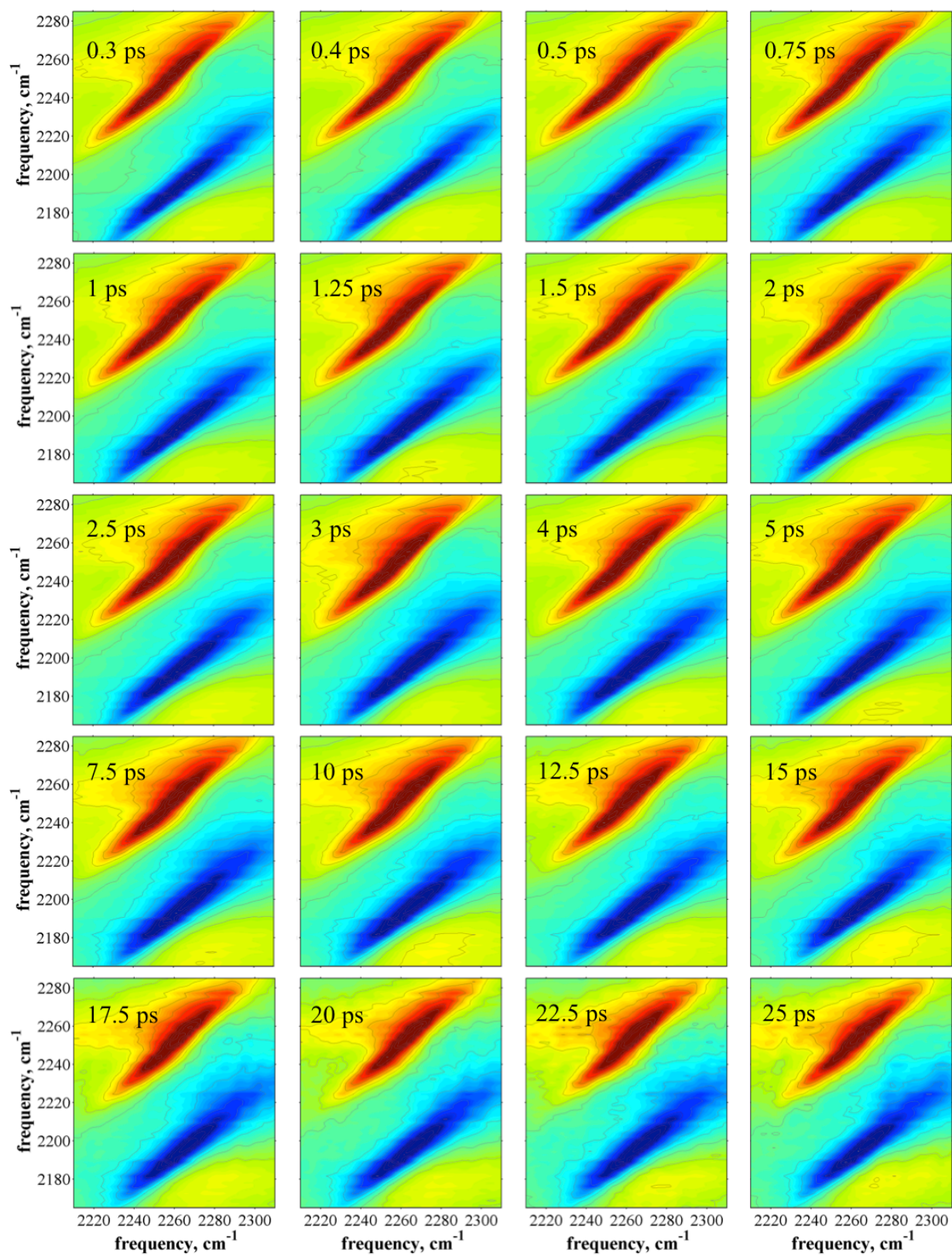**Figure S9.** 2D-IR spectra for DMF infiltrated alcogel.

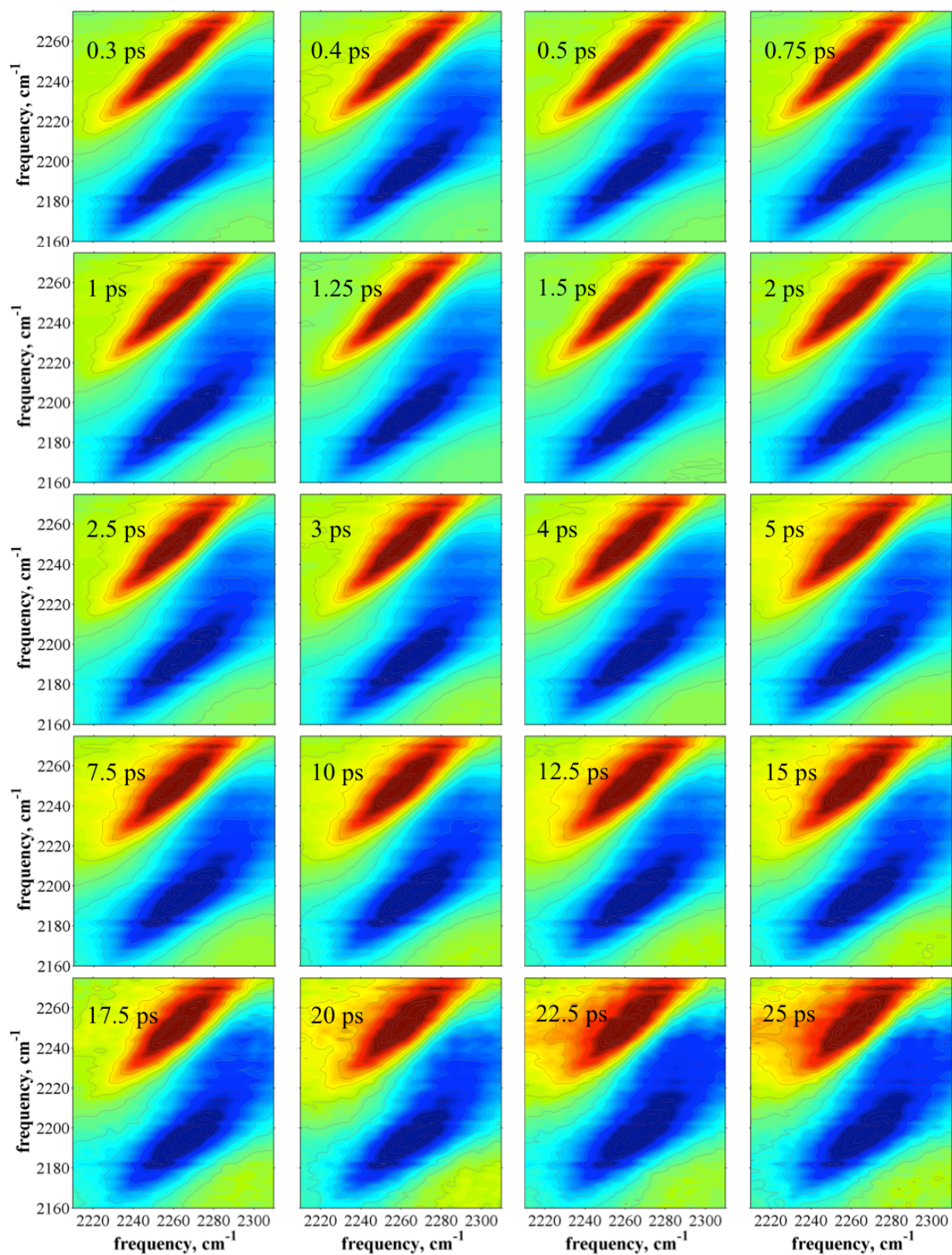**Figure S10.** 2D-IR spectra for chloroform infiltrated alcogel.

**Figure S11.** 2D-IR spectra for pentane infiltrated alcogel.

**Figure S12.** 2D-IR spectra for silica aerogel.

**Figure S13.** 2D-IR spectra for alcogel synthesized in isopropanol then switched to pentane.

**Table S2.** Vibrational lifetimes and exponential fit parameters to ellipticity decays for aerogel and alcogels.[a]

| sample | $T_1$ (ps) | $A_1$ | $\tau_1$ (ps) | $A_2$ | $\tau_2$ (ps) | y-intercept |
|---|---|---|---|---|---|---|
| aerogel | 14.4 (+/-0.4) | 0.017 (0.007) | 1.9 (2.0) | 0.939 (0.007) | 2060 (1820) | 0.956 |
| pentane | 12 (+/-0.7) | | | 0.950 (0.002) | 337 (34) | 0.950 |
| chloroform | 13.9 (+/-0.7) | 0.043 (0.003) | 1.2 (0.2) | 0.926 (0.002) | 408 (25) | 0.968 |
| DMF | 10.7 (+/-0.6) | 0.030 (0.002) | 4.1 (1.0) | 0.888 (0.002) | | 0.918 |
| isopropanol | 11.6 (+/-0.3) | 0.886 (0.008) | 449 (100) | 0.031 (0.008) | 1.9 (1.2) | 0.917 |

a. Errors shown in parentheses represent the standard error of the fit.

**Table S3.** Complete $C(t)$ parameters from ellipticity decays and iterative fitting of the linear lineshape for alcogel that began in isopropanol and then exchanged solvent to pentane.

| sample | $T_2$ (ps)[a] | $\Gamma$ (cm$^{-1}$)[a] | $\Delta_1$ (cm$^{-1}$)[a] | $\tau_1$ (ps)[b] | $\Delta_2$ (cm$^{-1}$)[a] | $\tau_2$ (ps)[b] |
|---|---|---|---|---|---|---|
| isopropanol to pentane | 2.8 (+0.6/-0.4) | 3.7 (+0.8/-0.6) | 3.9 (+/-0.3) | 2.7 (+/-2.4) | 23.6 (+/-19.4) | 373 (+/-91) |

a. Error values in parentheses for $T_2, \Gamma, \Delta_1$, and $\Delta_2$ represent iteratively determined parameter limits that allow 99% of the best-fit chi-squared value to be recovered by floating all other parameters.
b. Error values for $\tau_1$ and $\tau_2$ represent the standard error of the exponential fit to the ellipticity decay data.
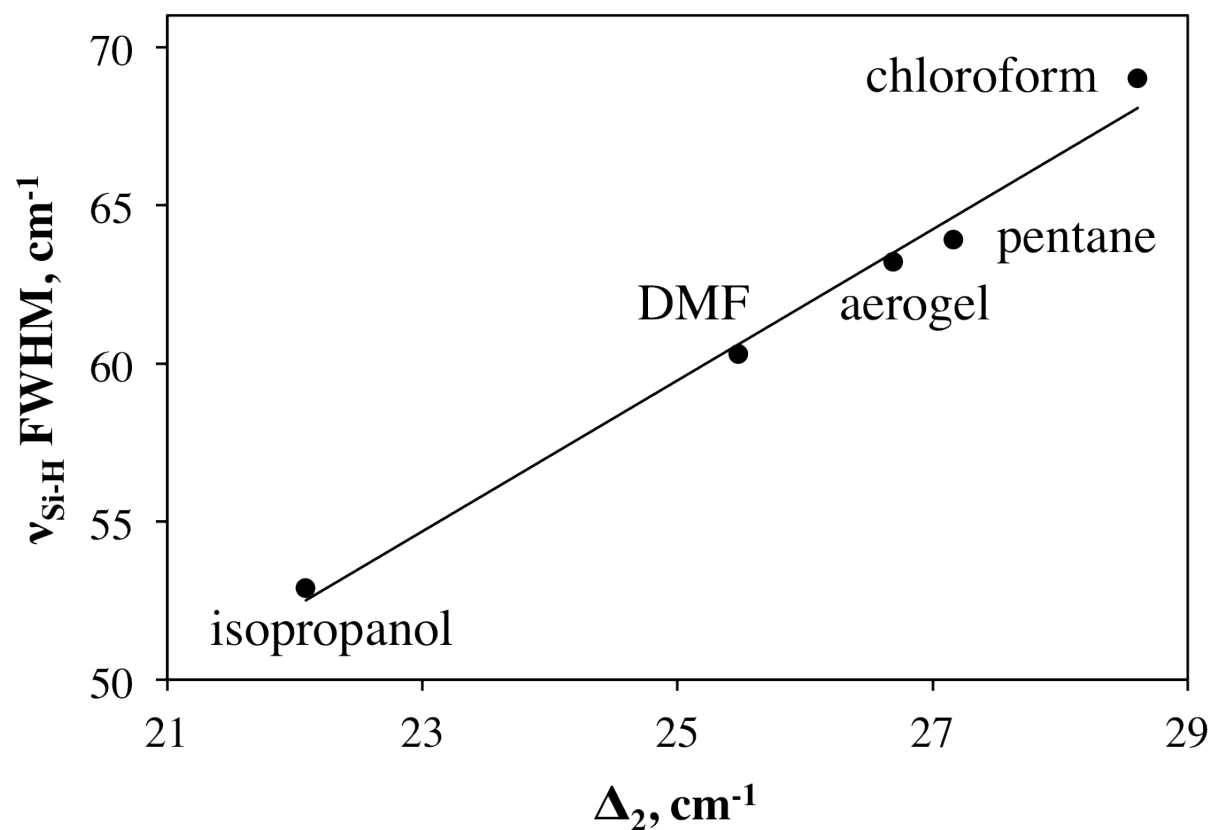
**Figure S14.** FWHM of the FTIR lineshapes of the $\nu_{\text{Si-H}}$ in the four alcogels and aerogel as a function of the static (or pseudo static) amplitude ($\Delta_2$) in the complete $C(t)$. The fact that there is a linear correspondence shows that the variations in the linear linewidth are due to increases in inhomogeneity, not dynamical differences.

## References

1.      I. S. Chuang and G. E. Maciel, *J. Phys. Chem. B*, 1997, 101, 3052-3064.

2.      L. W. Kelts and N. J. Armstrong, *J. Mater. Res.*, 1989, 4, 423-433.

3.      A. Steel, S. W. Carr and M. W. Anderson, *Chem. Mater.*, 1995, 7, 1829-1832.

4.      Y. Marcus, *Chem. Soc. Rev.*, 1993, 22, 409-416.

5.      J. Li, Y. Zhang and P. W. Carr, *Anal. Chem.*, 1992, 64, 210-218.